Colloidal microdynamics: Pair-drag simulations of model-concentrated aggregated systems

L. E. Silbert,[1,*] J. R. Melrose,[1] and R. C. Ball[2]
[1]*Polymers & Colloids Group, Cavendish Laboratory, University of Cambridge, Madingley Road, Cambridge CB3 0HE, United Kingdom*
[2]*Theory of Condensed Matter Group, Cavendish Laboratory, University of Cambridge, Madingley Road, Cambridge CB3 0HE, United Kingdom*
(Received 23 August 1996; revised manuscript received 2 September 1997)

We report results of simulations of a model for concentrated aggregated colloidal dispersions under shear flows. In an effort to study trends in rheology for varying colloidal interactions, we study a reduced hydrodynamic, frame-invariant, pair-drag model in which a long-range, many-body mobility matrix is generated just from resistance pair-drag terms that include lubrication. The model also includes depletion interactions, repulsive surface forces, and Brownian forces. We consider the steady-state rheology of the model which we varied in volume fraction between 30% and 53%. We are able to fit our data to experimental results. The rheology of the model is that of a power-law shear-thinning fluid with relative viscosity scaling with shear rate as $\eta_r \sim \dot{\gamma}^{-\alpha}$ and an exponent close to universal over a range of particle volume fractions 0.45–0.53. We also obtained a shear-thinning exponent that appears to be just weakly sensitive to the hydrodynamic model. The exponent α varies from 0.75 ± 0.02 for weakly aggregating systems to 0.86 ± 0.03 in the case of strong aggregating systems and the experimental data. As we lower the volume fraction we find a model-dependent transition to shear banding, where the rheology is effectively lost. We also find evidence of transitions between different shear-thinning regimes at the higher volume fractions when the particles are arranged in the familiar strings phases. [S1063-651X(97)13212-3]

PACS number(s): 47.50.+d, 83.50.−v

I. INTRODUCTION

Aggregated colloidal suspensions show a variety of non-Newtonian rheological properties, such as yield stress, shear thinning, shear thickening, thixotropy, and rheopexy [1]. Even at moderate concentrations, aggregating suspensions become ''gel-forming'' networks, considered to consist of continuous or percolating networks of particle aggregates prior to settling (sedimentation) [2], and are widely regarded as ''colloidal gels'' akin to polymeric systems [3]. In these microstructural fluids, the suspended particles interact through interparticle (conservative), hydrodynamic, and Brownian forces. Under equilibrium conditions, it is the competition between the interparticle and Brownian forces that determines the microstructures. However, when a shearing motion is introduced into the system, hydrodynamic forces must also be considered along with the interparticle and Brownian interactions. This highly nonequilibrium state raises many interesting questions about the microstructural organization under the influence of shear flows and the subsequent rheology of such systems. However, theoretical progress is hampered by the lack of insight into structural mechanisms.

Computer modeling is seen by many to be a route forward, but despite considerable effort, accurate algorithms for modeling the flow of particles concentrated in a hydrodynamic medium [4–7] are not yet efficient enough to allow studies far from equilibrium on relatively large systems across a parameter space of colloid interactions. Some authors [8,9] have simply dropped hydrodynamic interactions from their models in an attempt to gain some insight, although these algorithms are often physically naive representations of true systems. The simulations presented here offer an improvement on the nonhydrodynamic models by incorporating a computationally efficient, but approximate, hydrodynamic model that respects some, but not all, of the correct physics of these interactions under shear flow. It includes the leading-order terms in the mobility matrix in the limit of concentrated systems and should therefore be seen as a strong-coupling approximation; full details are given elsewhere [10]. We emphasize that our aims at this stage are to study trends in colloid rheology and to motivate new theory.

At lower concentrations than those of interest here, there are many theoretical models of the shear behavior of aggregates [11–15]. All these theories make untested assumptions about the microstructural behavior of the dispersion. However, a common ingredient in most of these theories is the idea that the stress in an aggregated system is carried through an open network that consists of the whole aggregate. The subsequent rheological behavior comes from the gradual breakdown in length scales over which the stress is carried, for example, breakup of fractal networks; see Ref. [14]. These assumptions can be effectively assessed by computer modeling. Our recent studies on the microstructural evolution of stress-bearing networks in concentrated, aggregating colloids [16] suggest that within the bulk there are dominant stress pathways consisting of rodlike particle structures. The resulting rheological behavior can then be described in terms of the rupture and reformation of these clusters [17].

Most of the simulations to date have involved models *without* hydrodynamic interactions employing the free-draining approximation [9,13,18–20]. At this level, Melrose and Heyes [9] performed simulations on flowing aggregates

*Electronic address: 1s10009@phy.cam.ac.uk

where they predicted gross structural changes under shear involving layering. In the models without hydrodynamic interactions, close particles do not feel divergent viscous interactions under relative motion. Shear is applied by coupling the particles to a background affinely shearing fluid which they do not disturb. These one-particle drag terms determine that the model is not Galilean invariant, and so-called mean-field hydrodynamics [8] as formulated does nothing to correct this failing. Limited studies have been made on the stresses of static aggregates by shear flow that do include hydrodynamic interactions [21–23] via low terms in moment expansions.

Hydrodynamic interactions must be important in real systems. Several methods have been proposed for accurately computing hydrodynamic interactions [4–7] and research continues. Moment expansions are [5] $O(N^3)$ in the number of particles N, to compute the motion at one time step, although an $O(N^2)$ method without Brownian forces has been proposed [4]. None of these methods has yet been shown to be computationally feasible for large systems with colloid interactions. The lattice Boltzmann [7] method has not been implemented with the moving boundary conditions required to impose shear flow and would need fine meshes to catch the divergent interactions between particles. Less accurate methods have been studied [24,25], the most extensively applied being that of Bossis and Brady [24]. However, the method is $O(N^3)$, and results for dynamic simulations of only small systems in three dimensions (3D) have recently been published. The method of Ref. [25] fails to handle close particle surfaces above 40% volume fraction and has not yet been developed with colloidal interactions.

We argue that the lowest-order approximation that retains much of the physics of hydrodynamic interactions is in the strong-coupling limit of concentrated systems—a *frame-invariant pair-drag model* with divergent lubrication interactions.

The equations of motion are given by a balance of forces/torques calculated as a sum over all nearest-neighbor pairs of hydrodynamic, conservative (colloid) forces, and random Brownian forces:

$$-\mathbf{R}\cdot\mathbf{V}+\mathbf{F}^C+\mathbf{F}^B=\mathbf{0}, \tag{1}$$

where $\mathbf{R}$, $\mathbf{F}$, and $\mathbf{V}$ denote a $6N\times 6N$ drag matrix and $6N$ force and velocity vectors, respectively. We deal first with the need for frame invariance. The hydrodynamic forces/torques on the particles can be viewed in matrix form as $\mathbf{U}=\mathbf{M}\cdot\mathbf{F}_H$ or, equivalently, $\mathbf{F}_H=\mathbf{R}\cdot\mathbf{U}$, where, in principle, $\mathbf{U}$ is a vector of fluid and particle velocities. In the absence of an explicit fluid velocity field in the simulation, we argue that it is physically incorrect to break frame (Galilean) invariance in the particle velocities; we therefore build the interaction model out of Galilean-invariant dissipative interactions, that is, the matrix $\mathbf{R}$ has the symmetry

$$\mathbf{R}\cdot(\mathbf{V}+\mathbf{U}_{\text{const}})=\mathbf{R}\cdot\mathbf{V}, \tag{2}$$

where $\mathbf{U}_{\text{const}}$ is a constant velocity field or a rigid rotation. The frame-invariant formulation implicitly assumes that in the problem of interest, the average fluid flow field is the same as the average particle velocity field, so such a formulation therefore cannot model many problems such as sedimentation. For a shear field Γ we rewrite (1) in the form

$$-\mathbf{R}\cdot(\mathbf{V}-\mathbf{V_0})+\mathbf{F}^C+\mathbf{F}^B-(\mathbf{R}\cdot\mathbf{V_0})=\mathbf{0}, \tag{3}$$

where $\mathbf{V_0}$ are a set of velocities defined at the particle centers by Γ with Lees-Edwards [26] (i.e., shear periodic) boundary conditions. By imposing periodic boundary conditions on the velocity difference $\mathbf{V}-\mathbf{V_0}$, we thus impose overall shear globally on our sample without locally constraining the flow.

We now discuss the long-range nature of hydrodynamics in a concentrated system and argue that a long-range mobility matrix can be formed from pair, near-field resistance terms. It is not generally recognized that one must carefully distinguish between the long-range nature of $\mathbf{M}$ and the much shorter range of $\mathbf{R}$. Consider **M:** elements of this can be interpreted in terms of the following thought experiment. Apply a unit force to one particle and measure the corresponding particle velocities under conditions in which they are force-free. Approximating the suspension as a fluid of viscosity η_T leads us to estimate the translational elements of $\mathbf{M}$ as

$$\mathbf{M}_{ij}\approx 1/(\eta_T r_{ij}) \quad \text{except} \quad \mathbf{M}_{ii}\approx 1/(\eta_T d), \tag{4}$$

where r_{ij} is the center-to-center separation of particles i and j, and d is a particle diameter. The key features of $\mathbf{M}$ are that it falls off as a slow power of distance and all elements are scaled by the same amplitude η_T.

The thought experiment for the elements of $\mathbf{R}$ is to give one particle unit velocity while holding all the others fixed, then measuring the forces on the particles. In concentrated systems, the near-neighbor (NN) and diagonal terms are dominated by lubrication effects and diverge at small interparticle gaps as

$$\mathbf{R}_{ij}\approx\frac{-\eta_0 d^2}{(r_{ij}-d)} \quad \text{for } r_{ij}\approx d \quad \text{and} \quad R_{ii}\cong-\sum R_{\text{NN}}, \tag{5}$$

whereas the longer-range elements of $\mathbf{R}$ can be estimated by analogy with a porous medium and give

$$\mathbf{R}_{ij}\approx\frac{-\eta_0 d^4}{r_{ij}^3}, \quad r_{ij}\gg d \tag{6}$$

(this can be seen from the Green's-function solution of the Brinkman equation and by theory including many-body interactions). The long-range part of $\mathbf{R}$ falls off as a much steeper power than for $\mathbf{M}$ and, moreover, the divergence with close interparticle gaps enters into the diagonal and nearest-neighbor terms but not the long-range terms.

For concentrated systems we find it compelling to exploit the dominance in the resistance matrix of the nearest-neighbor and diagonal terms (for which the dominant squeeze modes diverge as the interparticle gap and at that level are pairwise additive), over the longer-range terms, which have nondiverging amplitude and (compared to $\mathbf{M}$) relatively rapid falloff with distance. Inverting $\mathbf{R}$ to obtain $\mathbf{M}$, it is evident in concentrated systems, as the gaps become small, that the leading behavior of all the mobility elements comes exclusively from the nearest neighbors and diagonal terms of $\mathbf{R}$. In our earlier discussion of $\mathbf{M}$ [cf. Eq. (4)], this leading behavior, proportional to the interparticle gaps, is hidden in the factors η_T^{-1}.

The algorithm below identifies nearest neighbors and forms **R** pairwise out of terms including the divergent parts found in the lubrication approximation. Inversion of the sparse matrix **R** is performed by iterative techniques. As has often been stated, hydrodynamic simulations need to properly include the many-body and long-range nature of **M**, and the approximation at high concentrations includes the leading-order terms to this. However, it is an inaccurate approximation to the full hydrodynamic matrices, since it ignores local N-body effects in **R** itself in which the flows within the narrow gaps are coupled to the flows in the local pore space around the particle. Indeed, relative tangential (or shearing) motion has a coefficient diverging only as $\ln[d/(r_{ij}-d)]$ and although we include this in the computations, it is, in practice, not much more significant than the more distant elements of **R**, which we neglect.

Other workers are reporting pair-drag models [27] that include additional terms that break Galilean invariance. To be clear, we will refer to the model used here as a *frame-invariant, pair-drag* model.

We compare our simulation studies with recent experimental results on relatively well controlled weakly aggregated systems [28,29]. In particular, Buscall, McGowan, and Morton-Jones [28] carried out work on depletion-flocculated systems where the colloid particles had a thermodynamic volume fraction of 47%, through the combination of the hydrodynamic volume fraction of 40% plus the presence of a polymer-coated surface. Aggregation is induced through the addition of a nonadsorbing polymer into solution. The resulting osmotic imbalance arising from the exclusion of the polymer particles from a region around close-approaching colloid particles then leads to an effective attractive-well potential interaction, which depends on the size ratio of the two species and the concentration of the polymer particles. The resulting experimental attractive-well depths were estimated to lie between $-2.5k_BT$ and $-25k_BT$. However, the colloid particles are stabilized from coagulation in the deep primary minimum at very close contact (van der Waals minimum, $U_{\min}<-100k_BT$), through the inclusion of the surface polymer coat.

There are many ways to induce particle aggregation [30], but in an attempt to model depletion interactions, in our simulations we approximate the aggregating potential as that proposed by Asakura and Oosawa [31]. In the simulations, these weak aggregating forces provide an attractive interaction of the order of $-10k_BT$. In an attempt to model polymer-coated spheres, we include a steep repulsive spring force at the surface of our particles. This spring force effectively mimics the osmotic part of the polymer coat. These latter forces are neglected in most theories, but actually turn out to play a significant role in the simulations. However, all other aspects of this layer and interactions with the polymer species in solution are ignored. In particular, the viscous interactions due to the drainage of solvent through the polymer layer are neglected here.

There are several recent publications containing details of the simulation method, both carried out at the Rouse level [8,32] and those which include detailed hydrodynamic interactions [10,33]. Full and explicit details of our algorithm are presented elsewhere [10], so only a brief overview of the technique of the present simulations is presented in the next section. Section III focuses on the results obtained from the simulation studies.

II. SIMULATION METHOD

We consider time scales long with respect to the viscous momentum relaxation time of the suspension so that we treat the particles at the Langevin-Smoluchowski level and the fluid by the creeping-flow equations. Stick boundary conditions are imposed on the fluid at the particle surfaces. For N such particles, immersed in a Newtonian fluid with viscosity μ and density ρ, the equations of motion are described by the coupled N-body Langevin equation expressing force balance:

$$\mathbf{0}=\mathbf{F}^H+\mathbf{F}^P+\mathbf{F}^B. \tag{7}$$

The $6N$ force/torque vectors represent (i) the hydrodynamic forces $\mathbf{F}^H$ exerted on the particles due to their motion relative to the fluid, (ii) the interparticle forces $\mathbf{F}^P$, and (iii) the random Brownian forces $\mathbf{F}^B$.

A. Interparticle forces

The interparticle interactions include the contribution from the depletion interaction whose attractive force $\mathbf{f}^{\mathbf{A}}$ is approximated by [31]

$$\mathbf{f}^{\mathbf{A}}(r_{ij})=-\frac{Qk_BT}{d}[L^2-(r_{ij}/d)^2]H(Ld-r_{ij}), \tag{8}$$

where $L=1+\alpha/d$, with d being the diameter of the colloid particle, α twice the radius of gyration of the added polymer species at a volume fraction ϕ_p, r_{ij} the separation between the ith and jth particles, and $H(x)$ a unit step function.

The interaction strength Q depends on the volume fraction of polymer ϕ_p and the size ratio of this added polymer to the colloid particle α/d:

$$Q=\frac{3\phi_p}{2(\alpha/d)^3}. \tag{9}$$

For a typical ratio of α/d, and a sensible value for ϕ_p, Q ranges between 1000 and 10 000.

We use linear springs as the crudest model of conservative, repulsive forces between the adsorbed polymer coats. The repulsive force $\mathbf{f}^{\mathbf{R}}$ between spheres i and j separated by r_{ij} is

$$\begin{aligned}\mathbf{f}^{\mathbf{R}}(r_{ij})&=-\mathbf{n}_{ij}\frac{k_BT}{d}\{F_0-(F_0/\delta_c)(r_{ij}-d)\}\\ &\qquad \text{for } (r_{ij}-d)<\delta_c,\\ &=\mathbf{0}\qquad \text{for } (r_{ij}-d)>\delta_c.\end{aligned} \tag{10}$$

The Hookean spring coat thickness $\delta_c/2$ sets how much the *thermodynamic* size of the particle exceeds the *hydrodynamic* size of the particle. The term F_0 sets the maximal force the spring can supply and is set to 10^4 for all simulations.

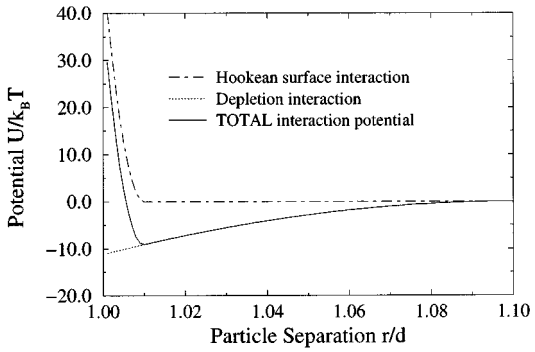

FIG. 1. The equilibrium interaction potential between particle pairs experiencing the attractive depletion forces with repulsive forces approximated by a Hookean spring surface of thickness 0.005 particle diameters. Polymer concentration, $\phi p = 0.7$, polymer/colloid size ratio $\alpha/d = 0.1$ ($Q = 1050.0$).

Figure 1 shows the interaction potential arising from the combination of the depletion interaction together with the repulsive surface forces. In the simulations reported below, all distances are measured in terms of the particle diameter d, which, for convenience, is set to unity. The coat thickness parameter $\delta_c = 0.01d$, $\phi_p = 0.70$, and the size ratio $\alpha/d = 0.1$; consequently, for $Q \sim 1000$, the particles at rest are aggregated in well depths of order $-10k_BT$. Two systems at higher ϕ_p are also presented (Fig. 7).

B. Hydrodynamic interactions and equations of motion

The hydrodynamic model, as mentioned earlier introduces a resistance tensor **R**, a sparse matrix, acting between nearest neighbors such that the hydrodynamic force is given by [see Eq. (2)]

$$\mathbf{F}^H = -\mathbf{R}\cdot\mathbf{V}. \tag{11}$$

The **V** are the $6N$ velocities and angular velocities, and **R** is actually a $6N \times 6N$ particle-configuration-dependent matrix.

For the nearest-neighbor hydrodynamics drag we use the leading singular terms in the lubrication approximation, the most divergent being the squeeze mode. The other modes, arising from the shear and transverse motion of neighbors, are logarithmically divergent with respect to the gap. We also include terms due to higher orders in the gap expansion which are also logarithmically divergent [6,34]. *To leading order* in the intersurface gaps, the *squeeze-mode* force $\mathbf{f}_i^H$ on particle i is given by

$$\mathbf{f}_i^H = -\sum_j (3\pi\mu d^2/8h_{ij})\{(\mathbf{v}_i - \mathbf{v}_j)\cdot\mathbf{n}_{ij}\}\mathbf{n}_{ij}, \tag{12}$$

where μ is the viscosity of the solvent, d being the particle diameter, the sum is over nearest-neighbor particles j, h_{ij} is the gap between the surfaces, $\mathbf{n}_{ij}$ is the unit vector along the line of centers i to j, and $\mathbf{v}_i$, $\mathbf{v}_j$ are the particle velocities.

For many of the results below, we will study models with just the squeeze interactions. This approximation is justified as we find that the scaling relation between stress and shear rate for the rheology with just squeeze lubrication interactions is relatively insensitive to the hydrodynamic model used in the simulations—whether we include higher-order terms or other hydrodynamical modes, the scaling exponent remains approximately constant.

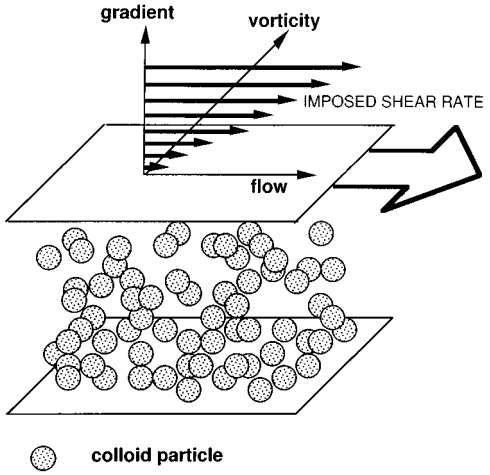

FIG. 2. The computational geometry of a single computational box for the simple shear-flow simulation, with the flow (x), gradient (y), and vorticity (z) directions (axes) defined as shown. The imposed shear rate is performed by Lees-Edwards boundary conditions across the top surface of the periodic boundaries.

Random forces and torques $\mathbf{F}^B$, when included, obey the fluctuation-dissipation theorem: $\langle \mathbf{F}^B\mathbf{F}^B\rangle = 2k_BT\mathbf{R}$. Including Brownian forces in the equations of motion is computationally expensive (e.g., fivefold for the typical data here). Solving for the particle motion, it is necessary to numerically solve Eq. (7) for the particle velocities **V**. Thus Eq. (7) becomes [cf. Eq. (1)]

$$-\mathbf{R}\cdot\mathbf{V} + \mathbf{F}^P + \mathbf{F}^B = 0, \tag{13}$$

which generates long-range correlations in the particle motion through the inversion of **R**, which has the computational merit of being sparse and is, in principle, an $O(N^2)$ operation, although we find that the practical scaling to achieve fixed accuracy is more like $N^{1.5}$ [10]. The flow is driven by Lees-Edwards boundary conditions [26] on systems in spatially periodic boundaries. The computational geometry is shown in Fig. 2, where the flow (x), gradient (y), and vorticity (z) directions (axes) are also defined.

In simulations of sheared aggregates when Brownian forces are neglected, the physics is solely determined by the competition between the colloid interactions and the shear forces. We introduce a dimensionless shear rate W, which is the single parameter determining the physics at a particular volume fraction. It is defined as the ratio of a shear force in the solvent in the absence of particles to the maximum attractive force of a particle-particle bond $f_{\max}(r)$ at a separation $r = d$:

$$W = \frac{F_{\text{shear}}}{f_{\max}(d)} = \frac{\mu d^2\dot{\gamma}}{Qk_BT/d}. \tag{14}$$

Here the dimensionless shear rate W is defined with respect to the solvent viscosity μ, d is the particle diameter, and Q has already been defined in Eq. (9). The choice of the definition of W is convenient in the following data plots. If

Brownian forces are included, W is related to the Peclet number, $\mathrm{Pe}=\mu d^3\dot{\gamma}/k_BT$ through the relation

$$W=\mathrm{Pe}/Q, \tag{15}$$

and all of the following rheology plots will be given in terms of the relative viscosity η_r of the bulk to that of the solvent and the dimensionless shear rate W. Since our studies are always at large Q ($Q>1000$), we are always in the phase-separating region. In W, we only vary the ratio of the shear forces to the colloidal forces. We do not vary the ratio of the Brownian forces to the colloidal forces, hence as we lower W, although Brownian forces will certainly become increasingly important relative to shear, the system remains in the phase-separating region in which colloid forces dominate over Brownian forces; see Fig. 6.

It must be noted that Eq. (14) involves only a crude estimate of the shear forces on a particle in the bulk suspension. The parameter $W'=\eta_rW$ will provide a more accurate estimation of the ratio of the bulk suspension forces to the aggregating forces, but η_r has to be computed from the simulation.

C. Computation of stress

The relative viscosity η_r, defined as the ratio of the suspension viscosity η to that of the solvent viscosity μ, can be calculated from the bulk stress of the suspension, defined by a sum over all nearest-neighbor interacting pairs:

$$\sigma=\frac{1}{\Omega}\sum_{ij}\mathbf{f}_{ij}\mathbf{r}_{ij}, \tag{16}$$

where $\mathbf{r}_{ij}$ is the edge vector and Ω is the volume of the computational box, and $\mathbf{f}_{ij}$ is the sum of the hydrodynamic [Eq. (12), for example] and intercolloid particle pair forces $(8)+(10)$. The Brownian contribution to the stress tensor is properly computed elsewhere [10,35]. Note that the shear-gradient-flow element of σ is the relative viscosity.

From the above definition of the relative viscosity and from Eq. (16) we obtain, for the total relative viscosity,

$$\eta_r=1+\eta_r^H+\eta_r^P+\eta_r^B \tag{17}$$

where the hydrodynamic, interparticle (sum of repulsive and attractive terms), and Brownian contributions to the relative viscosity are denoted as η_r^H, η_r^P $(=\eta_r^{P_R}+\eta_r^{P_A})$, and η_r^B respectively, and the unity contribution is that of the solvent.

D. Simulation strategy

The results presented here are for monodisperse spheres, whose initial random configurations were generated by Monte Carlo procedures. We formed configurations at rest without aggregating forces, and then turned on the shear and the aggregating forces together. As we will see below, Fig. 7, our simulations lie in the second half of the shear thinning region where much of any rest structure is lost. This procedure in the simulation is equivalent to those experiments of Hunter and Frayne [36] in which all structure was destroyed by high-flow treatments prior to low-shear studies. A number of simulations were carried out for each volume fraction studied encompassing a wide range of (dimensionless) shear rates ($10^{-2}<WQ<10^3$). For simulations carried out without Brownian forces, the time step was 0.002 in units where the shear rate and the particle diameter are both set equal to unity and we used a first-order time-step algorithm for moving particles. The typical number of time steps for runs were 100 000–200 000, with times to reach the steady state 20 000–50 000 steps. In the cases of simulations that included Brownian motion, we had to switch to a predictor-corrector algorithm with a variable time step ranging from 10^{-6} to 10^{-3}, and run for up to 10^6 time steps.

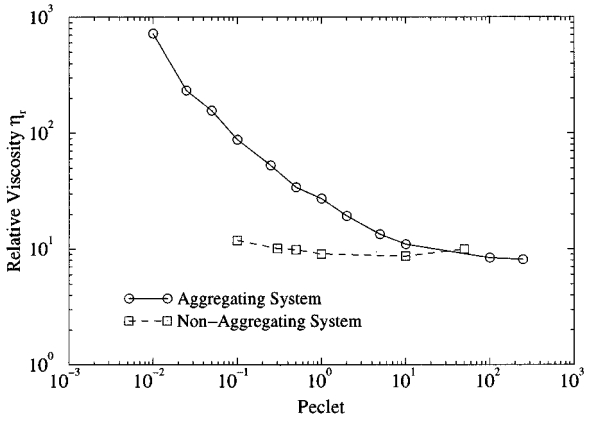

FIG. 3. Rheology at 45% volume fraction: a direct comparison between an aggregating system of Brownian spheres, which includes depletion interactions, with a system of nonaggregating, Brownian spheres, which has no aggregating forces. The aggregating system experiences an enhanced viscous response over the nonaggregating system.

III. RESULTS

There are two regimes of volume fraction to be considered. For volume fractions of 45% and above our systems exhibit shear-thinning behavior, which we are able to study and characterize in terms of shear stress and relative viscosity as a function of shear rate. We are able to examine the effects of volume fraction (Fig. 5), hydrodynamic force model (Fig. 6), and system size (Fig. 4) on the rheology of these systems. Over a large range of shear rates these systems obey that of a power-law, shear-thinning fluid (Figs. 5 and 6). At high shear rates we find evidence of a transition from the thinning regime (Figs. 5 and 9). We also investigate the dominant contributions to the stress tensor. We angularly decompose the stress contributions with respect to particle ''bond'' angle (Fig. 12).

By contrast, simulations at 40% volume fraction undergo shear banding and we effectively suffer a loss of rheology (Fig. 10). We present snapshots taken of particle configurations that show the structural organization that occurs when shear banding takes place (Fig. 9).

A. Rheology

We compare the simulation rheology data at 45% volume fraction, in Fig. 3, between Brownian spheres with aggregating forces to that of Brownian spheres without aggregating

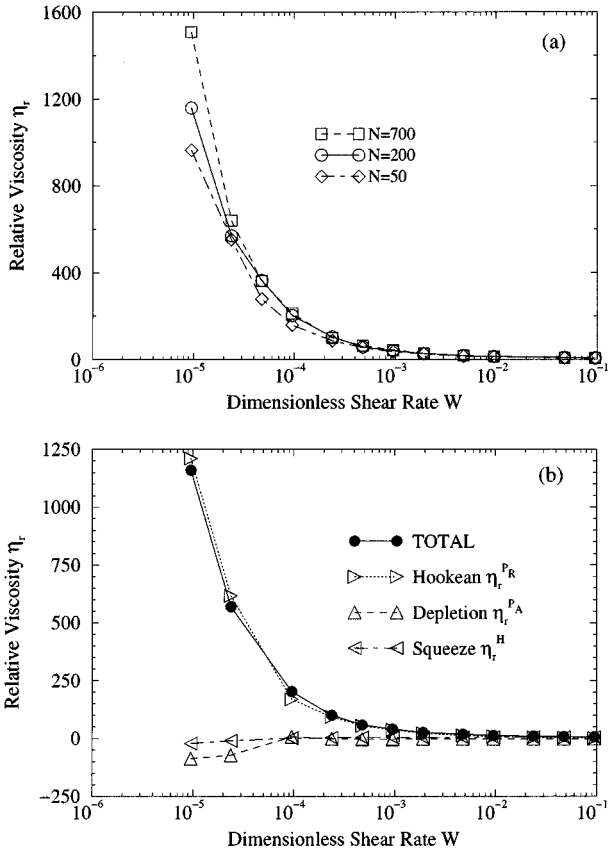

FIG. 4. Rheology at 50% volume fraction where the hydrodynamics is approximated by the squeeze lubrication terms and $U_{\min} = -9k_BT$: system size effects are investigated (a) for $N = 50$, 200, and 700 particles in a simulation cell. For the 200-particle system (b), contributions to the total viscosity are from the Hookean $\eta_r^{P_R}$, depletion $\eta_r^{P_A}$, and squeeze η_r^{H} forces, respectively.

forces. It is clear that the aggregating system experiences a large viscous enhancement over the nonaggregating system. In fact, their respective viscosities differ by an order of magnitude over the shear-thinning region. The presence of the aggregating forces results in extended structures within the bulk and an enhanced resistance to flow. Thus, the resultant behavior is an increase in viscosity over that of a non-phase-separating system.

Note that the system with just Brownian forces first shear thin and then thicken at higher shear rates. Due to the stiff coats, thickening behavior is not seen in our model aggregating system until we reach much larger shear rates, and then only to a very minor degree.

We show several rheology plots (Figs. 4–6) pertaining to several parameter changes in the simulations: volume fraction, hydrodynamic interactive models, and system size (number of particles and computational box size). In Fig. 4 the rheology plots at particle volume fraction 50% are shown. Figure 4(a) compares viscosity values for several system sizes, $N = 50$, 200, 700 particles per unit cell, whereas Fig. 4(b) displays the contributions to the total viscosity (for the system containing 200 particles).

The phase-separating systems experience an interaction potential-well depth of $-9k_BT$ due to the depletion forces, and are sheared until the steady-state regime is achieved over a wide range of shear rates. The total relative viscosity

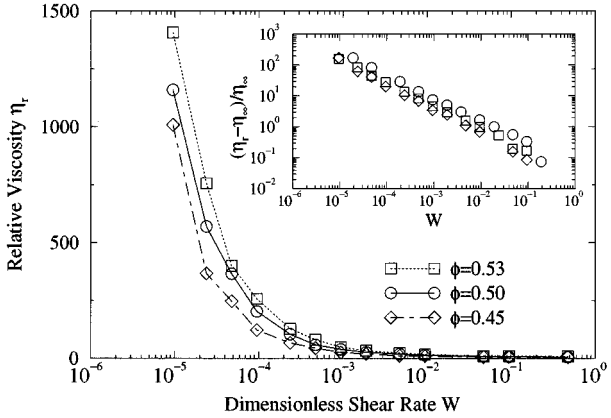

FIG. 5. The dependence of η_r, as a function of W, on $\phi(0.45 \leqslant \phi \leqslant 0.53)$ at the squeeze level of approximation for 200 particles. The inset shows how the scaled data collapses, resulting in the shear-thinning exponent $\alpha = 0.75 \pm 0.02$.

matches qualitatively experimental curves [28]: there is shear thinning over this range of W, with the high shear relative viscosity η_∞ being reached at the end of the shear-thinning curve. We only see shear thickening with this strength of aggregating force at the very highest shear rates (at 50%, $W = 1000/Q$). The curve has an effective plateau over a wide range of (high) shear rates. It is clear that system-size effects become increasingly pronounced as we lower the number of particles per unit cell. This can be explained due to limiting factors affecting the size of dominant, stress-bearing clusters [17].

The individual components contributing to the total relative viscosity, Fig. 4(b), demonstrate that the dominant contribution to the curve is that of the Hookean term (repulsive interparticle force contribution $\eta_r^{P_R}$). In contrast, the common ingredient in most theories is the stretching and breaking of elastic bonds; while this is certainly occurring, the results here suggest that over a range of concentrations studied (45–53 %), the dominant positive contribution to the viscosity comes from the compression of particle surfaces and/or coats. The depletion term (attractive interparticle force contribution $\eta_r^{P_A}$) contributes negatively overall to the viscosity, approaching zero as the end of the shear-thinning curve is reached. The squeeze term (hydrodynamic contribution η_r^{H}), however, changes sign from low to higher shear rates and then continues to rise gradually with increasing shear rate. The overall contributions from the squeeze and the depletion terms are negligible in comparison with the Hookean contribution throughout the shear-thinning region. At first sight, this is quite puzzling, as there is clearly an effect from the aggregating forces on the viscosity values—compare the aggregation viscosity data with that of the nonaggregating systems' results in Fig. 3. This will be further discussed below. The shear thickening is due to an increasing hydrodynamic contribution at the higher shear rates.

Figure 5 examines the variation of viscosity with volume fraction. Again, these simulations were carried out with the hydrodynamic interactions approximated by the squeeze term only and without Brownian forces. The aggregation potential has its minimum at roughly $-9k_BT$, and the compu-

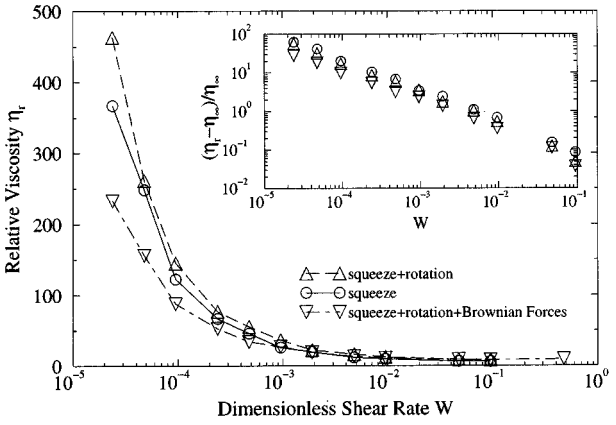

FIG. 6. η_r as a function of W at $\phi=0.45$ ($Q=1050.0$). The comparison is made between different hydrodynamic models. The squeeze-only model incorporates hydrodynamic interactions that act between particles whose relative velocities are directed along their line of centers. The squeeze and rotation model incorporates the squeeze terms as well as those lubrication interactions arising from the transverse motion of neighboring particles. Finally, the squeeze, rotation, and Brownian motion model includes the hydrodynamic modes as above with the inclusion of Brownian forces. The inset shows that the scaling between η_r and W is approximately unchanged with hydrodynamic model.

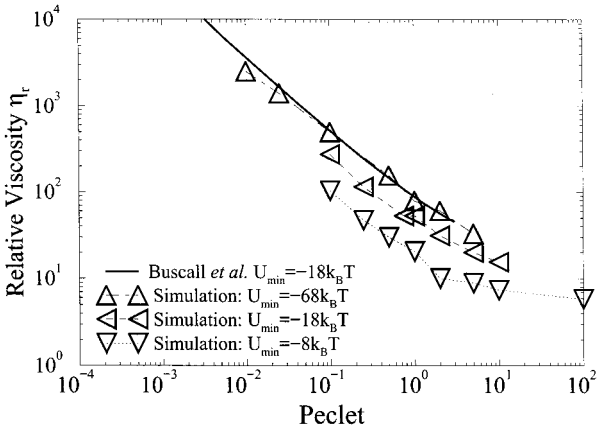

FIG. 7. Comparison of η_r for concentrated aggregating suspensions determined by simulation, with varying interaction well depths (open symbols), with well controlled experimental results by Buscall, McGowan, and Morton-Jones [28] with an estimated well depth of $-22k_BT$ (solid line). There is agreement only at the very deepest simulation well depth ($Q=7500$).

tational box contains 200 particles in all cases. Here we study three volume fractions, $\phi=0.45$, 0.50, and 0.53. As expected, the viscosity increases with increasing colloid concentration and each curve approaches a different value for η_∞, although this fact is not resolved on the scale of Fig. 5. For each volume fraction, each curve can be scaled with respect to its high-shear-rate viscosity. The inset shows the scaled data, for all three volume fractions, on a log-log plot.

We would anticipate that the full rheology curve might obey a Hershel-Buckely constitutive relation, but we do not shear at low enough rates to see the first Newtonian plateau. In the regime studied, the data obeys a Sisko [37] constitutive relation. When the viscosity is reduced according to this relation, the whole data set, for this range in volume fraction, collapses onto one curve (inset of Fig. 5). The shear-thinning exponent is calculated to be $\alpha=0.75\pm0.02$. This is indicative of a power-law fluid, with relative viscosity related to shear rate like $\eta_r\sim\dot{\gamma}^{-0.75}$. Thus we conclude that our systems behave as power-law, shear-thinning fluids with *universal* behavior over this range of volume fraction. The change in slope noticeable for $\phi=0.53$ (far right of inset) coincides with the ordering of particles into the string phase at these shear rates. See Sec. III B and Fig. 9.

We now test whether this behavior is independent (within the scope of the model) of the details of the hydrodynamic interactions included. This includes studies of aggregated systems where the hydrodynamics is approximated by only the squeeze terms, squeeze terms and rotational hydrodynamical modes, and finally squeeze and rotation hydrodynamics *and* Brownian forces. Figure 6 presents the rheology curves for these systems.

Again we see the expected occurrence of shear thinning and a leveling off at high shear rates as before. In comparing the effects of the details of the hydrodynamic model, we find that the inclusion of the rotation terms in the near-field approximation results in slightly higher computed viscosities (10–20 % increase over that of the squeeze-only simulations). These additional dissipative terms will lend additional variations in the local structures within the bulk and it is not unreasonable to expect slight variations in the viscous response of the system. The direct Brownian contribution to the viscosity is positive. However, at low shear rates in the regime where Brownian forces are non-negligible, the overall effect of the Brownian term is to lower the computed viscosities through the indirect effect it has on the viscosity contributions of the other forces, particularly the dominant Hookean term. The effect is to lower their computed values compared with those simulations that neglect Brownian forces. Physically, we reason that this is due to the effect Brownian forces have on the kinetics of the particle structures in the system. As mentioned above, aggregated systems under shear gain structural rigidity due to the extended particle networks that form as a consequence of the attractive forces between the particles. However, the effect of including Brownian forces is to disrupt these particle structures and enhance the rupture of the networks under shear, thus lowering the viscosity.

We see that from the scaled log-log plot, these variations in the model again collapse onto one curve. A fit of this line gives a value for $\alpha=0.78\pm0.04$. In general, we do expect the shear-thinning exponent to be sensitive to the model details [17], but within the scope of these studies the exponent appears to vary only within the margin of error.

We now pursue a direct quantitative comparison with the well controlled experimental work carried out by Buscall, McGowan, and Morton-Jones [28]. The experimental curve is for a system where the aggregating well depth was estimated to be $-18k_BT$ [28], and Fig. 7 shows simulation-data fits to this curve. We simulate systems with *weak* aggregating interaction potentials, $U_{\min}=-9k_BT$ ($Q=1050.0$), $U_{\min}=-18k_BT$ ($Q=3000.0$), and also strong aggregating interaction potentials, $U_{\min}=-68k_BT$ ($Q=7500.0$). We see that with our simple model, the simulation only fits the experimental data in the limit of very strong aggregating forces ($Q=7500.0$) which for the depletion potential is unphysi-

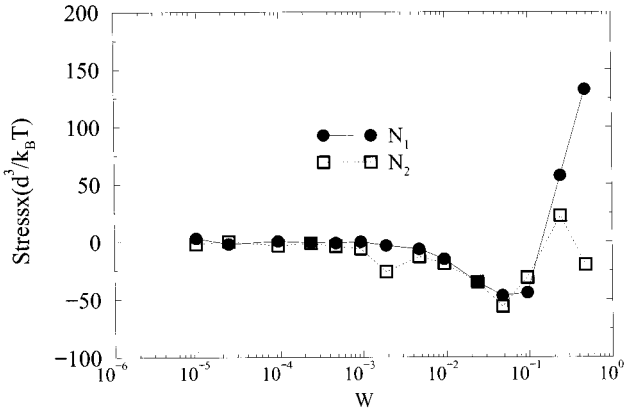

FIG. 8. Variation of the two dimensionless normal stress differences N_1 and N_2 with shear rate, for 200 particles at $\phi=0.50$. They both remain close to zero until high shear rates are reached. As the string phase is approached, both N_1 and N_2 dip, but as the strings begin to melt and the particle gaps collapse, N_1 becomes positive.

cally large—we will discuss this failing below. We note that there is, however, agreement between the simulation and experiment in the shear-thinning exponent, $a_{\text{expt}}=0.87\pm0.01$ compared with $\alpha_{\text{simulation}}=0.86\pm0.03$. At this high potential, the shear-thinning exponent is altered.

A normal stress-differences plot is shown in Fig. 8. This data is taken from a system at 50% volume fraction where the hydrodynamics is modeled on the squeeze interactions and an aggregating well depth of $-9k_BT$. The two normal stress differences, N_1 and N_2, are defined as [1]

$$N_1=\sigma_{xx}-\sigma_{yy}, \tag{18a}$$

$$N_2=\sigma_{yy}-\sigma_{zz}, \tag{18b}$$

where the shear flow imposed is in the x direction with gradient along the y direction. Initially the two dimensionless normal stress differences stay close to zero. It is questionable whether this is because there is no definable structure over this range of shear rate or because there exist isotropic structures in the flow. At intermediate shear rates $W=1/Q$, both N_1 and N_2 become slightly negative. At higher shear rates, the normal stress differences become markedly more negative, coincident with the initial formation of the string arrangement at this shear rate. N_1 then recovers and becomes positive. This last effect is due to the gradual melting of the string phase at the highest shear rates. The interparticle gaps begin to collapse and logarithmic shear thickening is seen. The generic shape of this curve is indicative of the change in the microstructure as the particles suffer increasing shear stresses.

B. Microstructure

1. Strings and bands

We now proceed to qualitatively investigate the microstructure under several flow conditions and shear rates. In line with the preceding subsection, Fig. 9 shows snapshots of particle configurations taken at 50% volume fraction, the same systems studied in Fig. 4. These systems contain 200

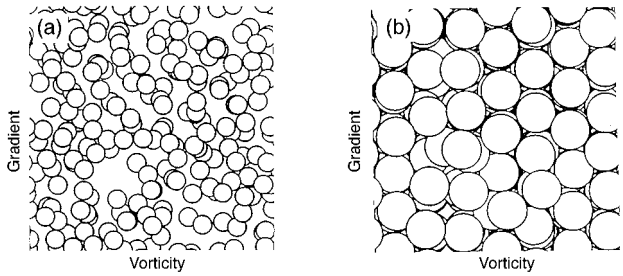

FIG. 9. Typical microstructural snapshots, taken looking down the flow direction, for systems at 50% volume fraction with 200 particles ($Q=1050.0$). (a) For $W<W_{\text{string}}$ ($W=1.0/Q$) the appearance is of a homogeneous distribution of particles with no obvious ordering (particles drawn at half size for clarity). (b) Above a certain shear rate W_{string} ($W=250.0/Q$), the particles flow in string formation (particles drawn at full size).

particles in a computational box. The structure looks homogeneous, in Fig. 9(a), until high shear rates are approached when the string phase is reached. These qualitative features suggest that the ordering of particles is not responsible for the shear-thinning effect. Figure 9(a) is taken halfway down the shear-thinning curve, whereas 9b) corresponds to a point on the right side of the rheology curve from Fig. 4. In the string phase, the particles flow in ''tubes'' aligned parallel to the imposed flow direction as in Fig. 9(b). The overall arrangement of these tubes is hexagonal.

At lower volume fractions, below 45%, there is a drastic change in the behavior of the model suspensions, effectively a loss of constitutive rheology. For the lower volume fractions studied here, 30–40 %, the systems tend to exhibit shear banding. An example of a banded configuration of 700 particles at shear rate $W=5/Q$ is shown in Fig. 10(a); as the shear rate is increased, the banded configuration is torn apart by the flow as shown in Fig. 10(b) at $W=100/Q$. Banding phenomena such as this are extremely interesting facets of complex fluids under flow. Others have found this kind of behavior in simulations of pressure-driven flows of hard-sphere suspensions [38]. Figure 11 shows the stress–shear-rate curve for the shear-banding system that follows qualitatively previously calculated curves [39]. The inset gives the typical velocity profile across the computational box for a banded system. Here the velocity profile for Fig. 10(a) is shown.

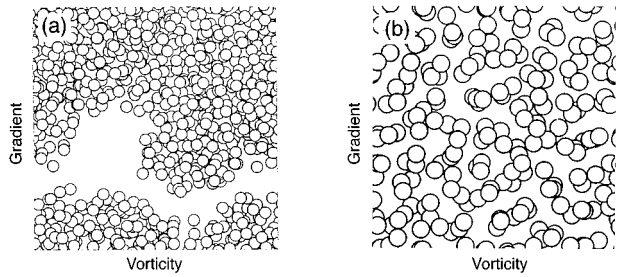

FIG. 10. Snapshots looking down the flow direction where the particles are drawn at half size at 40% for (a) a banded configuration of 700 particles at intermediate shear rates ($W=5.0/Q$); (b) 200 particles at high shear rates, where the banding has been broken up by the flow ($W=100.0/Q$).

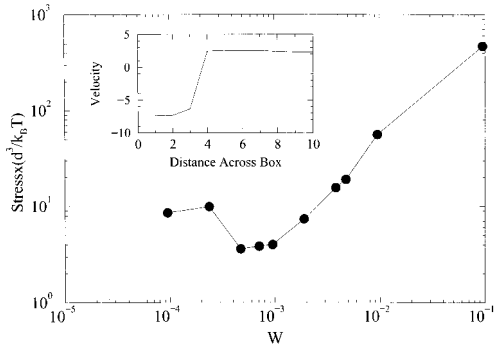

FIG. 11. Behavior of the stress with shear rate at 40% volume fraction where shear banding takes place over intermediate shear rates. The stress is nonmonotonic. The velocity profile, in units where the shear rate and particle diameter are both set to unity, across the box (bottom to top is left to right on the axis) for Fig. 10(a).

2. Angular decomposition of the stress tensor

Unlike many models, our particles are given a strong repulsive force on their surfaces which we found to make a dominant contribution to the shear stress. On the face of it, the attractive forces make a small contribution; yet, as the stresses are greatly enhanced over the case without the aggregating forces, this cannot in detail be the case. In this section we further analyze the different contributions to the stress to understand this dilemma. In Fig. 12, we plot the distribution of shear stress tensor per pair of interacting particles analyzed with respect to the orientation of the particle pair and the contributing interaction. For each interacting pair over many configurations, we projected the particle-center–to–particle-center vector onto the shear-gradient flow plane and resolved data according to the angle formed between the projected vector and the shear-gradient axis, the angle of 0° being parallel to the shear-gradient axis (see Fig. 2). The contributions to the stress tensor, as defined in Eq. (16), are shown, namely, the Hookean repulsive term, the depletion term, and the *squeeze* hydrodynamics term. What we find, in Fig. 12, is that the directions along which the Hookean and depletion contributions are largest are the shear-*compressional* and the shear-*extensional* directions, respectively. The Hookean term contributes highly *positively* to the viscosity along the *compressional* direction, but negatively along the extensional direction. However, their angular integral gives an overall dominant positive contribution to the viscosity, as shown in Fig. 4(b). In contrast, while the magnitude of the attractive contributions at each angle are individually of the same order of magnitude as the repulsive component and their signs are opposite, their angular integral is close to unity. The hydrodynamic squeeze force contributes both positively and negatively in both the extensional and compressional directions. This is possible because the squeeze interaction is dependent on the relative velocities of the particle pair. Overall, however, the squeeze force contributes positively to the total viscosity.

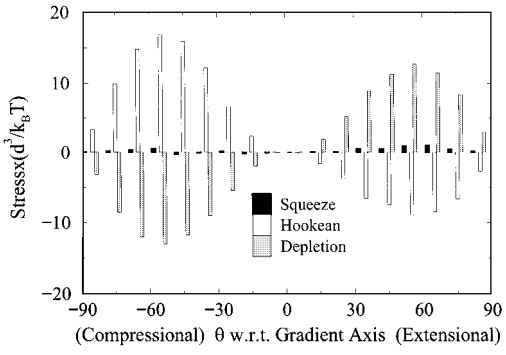

FIG. 12. Decomposition of the viscosity component of the stress tensor with respect to (w.r.t.) particle bond angle, with 0° being parallel to the shear-gradient axis. The contributions to the stress are the squeeze, Hookean, and depletion terms. The compressional and the extensional directions are seen to be dominant.

IV. SUMMARY AND DISCUSSION

We must emphasize that due to the reduced hydrodynamic interactions, the model may fail to represent well the physics of the real system. However, it is clear that the conservative colloid interactions dominate the stress, so the inaccurate estimates of the hydrodynamic contributions may not be significant in themselves. The neglect of fluid pumping in the general pore space around the particles is likely to be significant for aggregate deformations, but we assume this is not important at the concentrations studied. Of course, the true hydrodynamics may give qualitatively different particle flows.

Nevertheless, we do gain some insight from the model. We have seen how the inclusion of an aggregating potential greatly enhances the viscosity of a suspension compared with that of a nonaggregating system. It has been shown that for these concentrated systems there exists a regime of approximate universal power-law shear-thinning behavior over the range of volume fraction $0.45 \leqslant \phi \leqslant 0.53$ for weak aggregation potentials with exponents close to those of experiment. We note that these exponents vary only very slightly across different varieties of the model, in particular across what must be a significant qualitative change in the particle motions: turning the shear modes and particle rotation on and off. This is all, at least, *suggestive that the missing hydrodynamic features will not alter these exponents*. The exponents do, however, change for more strongly aggregating potentials.

The model failed to quantitatively predict the experiment unless unrealistically high potentials are introduced. This may be due to the missing hydrodynamic terms. However, this would require an order-of-magnitude-larger hydrodynamic contribution than that in the current model—we doubt that this is reasonable: if we estimate the full hydrodynamic contributions from that for Brownian hard spheres at the volume fractions and flow conditions of interest, this only increases the small hydrodynamic contribution in the results above by some 20–30 %. There is another important feature neglected in the model: the experimental particles have a polymer coat on their surfaces, and the aggregating forces determine that the particles will have these coats in contact. Contacting coats will greatly enhance the local viscous interactions between spheres [40]. We have made preliminary calculations which show that the viscosity values of the experiments can be computed with realistic potentials in the

range of the polymer coats and we will report on this in the near future [41]. A second reason may be that the real system feels the stronger van der Waals attraction, but evidence of a degree of irreversible aggregation on shear was not reported in the experiments of Ref. [28].

The model showed shear banding in systems at the lower volume fractions studied, $\phi \leqslant 0.40$. In such systems the stress is shown to be nonmonotonic with increasing shear rate. At rest our systems are phase separating; this is therefore a shear-induced orientation of thermodynamically driven separation rather than a shear-induced banding of a stable thermodynamic system. This may be a false prediction for a real colloid system because it is clear that it will be sensitive to the full hydrodynamics we have excluded. Since we approximate the hydrodynamic interactions between particle pairs as a pair drag, the gross separations that occur with shear banding call into question the validity of the model, and indeed we do find that the occurrence of shear banding is dependent on the details of the model. In particular, the inclusion of Brownian forces at 40% volume fraction with Brownian forces ''switched on,'' the systems *do not* shear band [Fig. 13(a)]; however, Figure 13(b) shows a system at 30% *with* Brownian forces switched on, and here we do see evidence of shear banding. Evidently, as we decrease the volume fraction there is an increased sensitivity to shear banding. From the theoretical point of view, a model showing shear banding is interesting *per se*. Shear banding has been studied, in a theoretical context, for polymers and wormlike micelles at high shear rates [39]. Symmetry suggests that bands may form in steady states normal to either the gradient direction or the vorticity direction. The orientation of shear banding in the model here (normal to the gradient direction) is not that found for free-draining models [9] (normal to the vorticity axis) at intermediate shear rates with the same potentials. This suggests that the orientation requires global application of the shear field—through true Lees-Edwards boundary conditions as above, and that it is sensitive to artificial coupling to a background affine flow field as in the free-draining model.

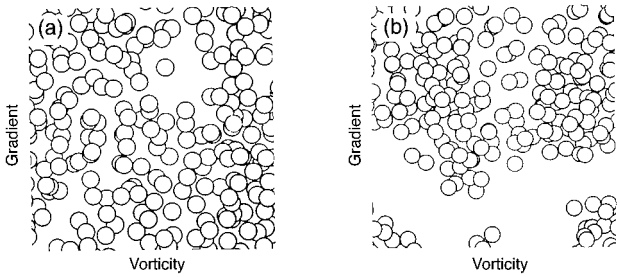

FIG. 13. Snapshots of 200 particles with Brownian motion included at (a) 40% compared with (b) banding at 30% (both at $W = 1/Q$).

Understanding the nature of concentrated aggregating systems under shear has been tackled here. We provide impetus for further work, including a theoretical challenge to elucidate the microstructural behavior of such colloidal systems [16,17], the role of surfaces [41], and shear-banding effects. Models far closer to physical systems than previous works [9,14,20] have been simulated, to a certain degree, showing behavior close to universal. More complete hydrodynamics and more realistic surface models are needed before comprehensive predictions can be made.

ACKNOWLEDGMENTS

We thank the DTI/Colloid Technology Project cofunded by the DTI, Unilever, Schlumberger, ICI, and Zeneca, the Colloid Hydrodynamics Grand Challenge Project, and the BBSRC food directorate, together with Dalgety plc. for funding.

[1] H. A. Barnes, J. F. Hutton, and K. Walters, *An Introduction to Rheology* (Elsevier, New York, 1989).
[2] For recent examples, see W.-H. Shih, W. Y. Shih, S-I. Kim, J. Liu, and I. A. Aksay, Phys. Rev. A **42**, 4772 (1990); H. Verduin, B. J. de Gans, and J. K. G. Dhont, Langmuir **12**, 2947 (1996).
[3] P-G. de Gennes, *Scaling Concepts in Polymer Physics* (Cornell University Press, Ithaca, 1979).
[4] B. Cichocki, B. U. Felderhorf, K. Hinsen, E. Wajnryb, and J. Blawzdziewicz, J. Chem. Phys. **100**, 3780 (1994), and references therein.
[5] A. J. Ladd, J. Chem. Phys. **93**, 3484 (1990).
[6] S. Kim and S. J. Karrila, *Microhydrodynamics* (Butterworths, London, 1992).
[7] A. J. Ladd, J. Fluid Mech. **271**, 285 (1994), and references therein.
[8] D. M. Heyes and J. R. Melrose, J. Phys. Condens. Matter **7**, 8857 (1995).
[9] J. R. Melrose and D. M. Heyes, J. Colloid Interface Sci. **157**, 227 (1993); J. R. Melrose and D. M. Heyes, J. Chem. Phys. **98**, 5873 (1993).
[10] R. C. Ball and J. R. Melrose, Physica A (to be published).
[11] T. G. M. van de Ven and R. J. Hunter, Rheol. Acta **16**, 534 (1977).
[12] R. J. Hunter, *Foundation of Colloid Science Vol. II* (Clarendon, Oxford, 1980).
[13] A. A. Potanin and W. B. Russel, Phys. Rev. E **53**, 3702 (1996); A. A. Potanin, R. De Rooij, D. Van den Ende, and J. Mellema, J. Chem. Phys. **99**, 9213 (1993); *ibid.* **102**, 5845 (1994), and references therein.
[14] R. Wessel and R. C. Ball, Phys. Rev. A **46**, R3008 (1992).
[15] P. Snabre and P. Mills, J. Phys. III **6**, 1811 (1996).
[16] L. E. Silbert, R. S. Farr, J. R. Melrose, and R. C. Ball (unpublished).
[17] R. S. Farr, L. E. Silbert, J. R. Melrose, and R. C. Ball (unpublished).
[18] M. Doi and D. Chen, J. Chem. Phys. **90**, 5271 (1989); D. Chen and M. Doi, *ibid.* **91**, 2656 (1989).
[19] F. E. Torres, W. B. Russel, and W. R. Schowalter, J. Colloid Interface Sci. **142**, 554 (1991).
[20] A. H. L. West, J. R. Melrose, and R. C. Ball, Phys. Rev. E **49**, 4237 (1994).

[21] G. Bossis, A. Meunier, and J. F. Brady, J. Chem. Phys. **94**, 5064 (1991).
[22] Z.-Y. Chen, J. M. Deutch, and P. Meakin, J. Chem. Phys. **80**, 2982 (1984); Z.-Y. Chen, P. C. Neakliem, and P. Meakin, *ibid.* **89**, 5887 (1988).
[23] P. Meakin, in *On Growth and Form*, edited by H. E. Stanley and N. Ostrowsky (Martinus Nijhoff, Dordrecht, 1986).
[24] G. Bossis and J. F. Brady, J. Chem. Phys. **80**, 5141 (1984); L. Durlofsky, J. F. Brady, and G. Bossis, J. Fluid Mech. **180**, 21 (1987); T. N. Phung, J. F. Brady, and G. Bossis, J. Fluid Mech. **313**, 181 (1996).
[25] J. M. V. A. Koelman and P. J. Hoogerbrugge, Europhys. Lett. **21**, 363 (1993); **19**, 155 (1992).
[26] A. W. Lees and S. F. Edwards, J. Phys. C **5**, 1921 (1972).
[27] M. Doi, D. Chen, and K. Saco, in *Ordering and Organising in Ionic Solutions* (World Scientific, Singapore, 1987), p. 482, M. Toivakka, D. Eklund, and D. W. Bousfield, J. Non-Newtonian Fluid Mech. **56**, 49 (1995).
[28] R. Buscall, J. I. McGowan, and A. J. Morton-Jones, J. Rheol. **37**, 621 (1993).
[29] P. D. Patel and W. B. Russel, Colloids Surface **31**, 355 (1988).
[30] W. B. Russel, D. A. Saville, and W. R. Showalter, *Colloidal Dispersions* (CUP, Cambridge, 1990).
[31] S. Asakura and F. Oosawa, J. Chem. Phys. **22**, 1255 (1954); J. Polym. Sci. **33**, 183 (1958).
[32] D. M. Heyes, Comp. Phys. Rep. **8**, 71 (1988); D. M. Heyes, J. Non-Newtonian Fluid Mech. **27**, 47 (1988).
[33] J. R. Melrose and R. C. Ball, Adv. Colloid Interface Sci. **59**, 19 (1995); J. R. Melrose and R. C. Ball, Europhys. Lett. **32**, 535 (1995); J. R. Melrose, J. H. van Vliet, and R. C. Ball, Phys. Rev. Lett. **77**, 4660 (1996).
[34] D. J. Jeffrey and Y. Onishi, J. Fluid Mech. **139**, 261 (1984).
[35] G. Bossis and J. F. Brady, J. Chem. Phys. **91**, 1866 (1989).
[36] R. J. Hunter and J. Frayne, J. Colloid Interface Sci. **76**, 107 (1980).
[37] A. W. Sisko, Ind. Eng. Chem. **50**, 1789 (1958).
[38] P. R. Nott and J. F. Brady, J. Fluid Mech. **275**, 157 (1994).
[39] N. A. Spenley, X. F. Yuan, and M. E. Cates, J. Phys. II **6**, 551 (1996).
[40] G. H. Fredrickson and P. Pincus, Langmuir **7**, 786 (1991); A. A. Potanin and W. B. Russel, Phys. Rev. E **52**, 730 (1995).
[41] L. E. Silbert, J. R. Melrose, J. H. van Vliet, and R. C. Ball (unpublished).